

Cite this: *Catal. Sci. Technol.*, 2020,
10, 7194Improving alkane dehydrogenation activity on
 γ -Al₂O₃ through Ga doping†Mona Abdelgaid,  James Dean  and Giannis Mpourmpakis *

Nonoxidative alkane dehydrogenation is a promising route to produce olefins, commonly used as building blocks in the chemical industry. Metal oxides, including γ -Al₂O₃ and β -Ga₂O₃, are attractive dehydrogenation catalysts due to their surface Lewis acid–base properties. In this work, we use density functional theory (DFT) to investigate nonoxidative dehydrogenation of ethane, propane, and isobutane on the Ga-doped and undoped (100) γ -Al₂O₃ via the concerted and stepwise mechanisms. We revealed that doping (100) γ -Al₂O₃ with Ga atoms has significant improvement in the dehydrogenation activity by decreasing the C–H activation barriers of the kinetically favored concerted mechanism and increasing the overall dehydrogenation turnover frequencies. We identified the dissociated H₂ binding energy as an activity descriptor for alkane dehydrogenation, accounting for the strength of the Lewis acidity and basicity of the active sites. We demonstrate linear correlations between the dissociated H₂ binding energy and the activation barriers of the rate determining steps for both the concerted and stepwise mechanisms. We further found the carbenium ion stability to be a quantitative reactant-type descriptor, correlating with the C–H activation barriers of the different alkanes. Importantly, we developed an alkane dehydrogenation model that captures the effect of catalyst acid–base surface properties (through dissociated H₂ binding energy) and reactant substitution (through carbenium ion stability). Additionally, we show that the dissociated H₂ binding energy can be used to predict the overall dehydrogenation turnover frequencies. Taken together, our developed methodology facilitates the screening and discovery of alkane dehydrogenation catalysts and demonstrates doping as an effective route to enhance catalytic activity.

Received 23rd July 2020,
Accepted 9th September 2020

DOI: 10.1039/d0cy01474e

rsc.li/catalysis

Introduction

Olefins are important chemical building blocks employed in the production of a vast array of commodity chemicals such as polymers, plastics, and petrochemicals.^{1–3} Traditionally, the production of these building blocks relies on crude oil fractionation, with steam cracking and fluid catalytic cracking dominating in the olefins production industry.^{1–6} However, such methods suffer from serious drawbacks including the use of nonrenewable fossil fuels, and the intensive energy requirements (elevated temperatures of 500–700 °C and high pressures of 5–70 bar) alongside the unavoidable side reactions and poor olefin selectivity and yield.^{1–6} These challenges in addition to the increasing gap between global olefin demand and supply, led to a surge in research toward

identifying economic and efficient chemical processes for olefins production.

Light alkanes are present in the abundant shale gas reserves, making them an inexpensive raw chemical.^{1–3} As a result, catalytic dehydrogenation of light alkanes on metal oxides is an attractive route to produce olefins.^{1,2} Catalytic alkane dehydrogenation can be categorized into nonoxidative alkane dehydrogenation (ADH) and oxidative dehydrogenation (ODH). The latter is an exothermic reaction and requires an oxidant, such as O₂ and CO₂.^{3,4,7} Although ODH is an attractive option from a thermodynamics perspective, it suffers from limitations including: (i) low olefin selectivity/yield due to the unavoidable over-oxidation (combustion) of the reacting alkane to CO_x products and (ii) the explosive nature of certain feed compositions due to the presence of oxygen.^{4,8,9}

Contrary to ODH, ADH is an endothermic and equilibrium-limited reaction that requires energy-intensive operating conditions, characterized by high temperatures and low pressures to obtain a high yield of olefins.^{1–4,8,9} The olefins in the resulting gas mixture stream are separated from residual hydrogen and other side products. The resulting hydrogen could be potentially combusted for

Department of Chemical Engineering, University of Pittsburgh, Pittsburgh, PA 15261, USA. E-mail: gmpourmp@pitt.edu

† Electronic supplementary information (ESI) available: Structure of surface facets of γ -Al₂O₃; energy profiles for propane and isobutane dehydrogenation; plots of dehydrogenation barriers vs. H₂ BE; H₂ production barriers vs. CIS for the stepwise mechanism; tables of model parameters, and turnover frequencies. See DOI: 10.1039/d0cy01474e

heating the reactor, thus eliminating the need for an additional fuel source.⁴ In ADH, all equivalent C–H bonds in the reacting hydrocarbon have an equal chance to participate in the reaction.¹⁰ Therefore, an effective catalyst that is both selective and active is required to avoid side reactions that include coke formation and undesired thermal cracking of the feedstock and products.^{3,4} Metal oxides can activate C–H bonds of alkanes due to their characteristic Lewis acidity (metal) and basicity (oxygen).^{1,11–23} Recently, group IIIA metal oxides, such as gallium oxide and aluminum oxide, have shown promise for ADH.^{1,2,7,11,23} Out of the different five gallium oxide polymorphs, monoclinic beta phase (β -Ga₂O₃) is the most chemically and thermally stable.²⁴ β -Ga₂O₃ is found to be highly active in the initial stages of the dehydrogenation reaction, however, the activity of β -Ga₂O₃ decreases quickly within an hour.⁷ Liu *et al.* investigated propane dehydrogenation on (100) β -Ga₂O₃ by using first principles methods. Two C–H bond activation mechanisms, concerted and radical (gas and surface stabilized), were considered, with the radical pathway being energetically preferred.⁷ Pidko *et al.* computationally investigated ethane dehydrogenation over gallyl ions (GaO⁺) stabilized in ZSM-5 zeolite. The authors revealed that GaO⁺ ions cannot be considered as the active sites in light alkane dehydrogenation over oxidized Ga/ZSM-5 zeolites because these ions are reduced quickly to Ga⁺ ions.²⁵

γ -Al₂O₃ is one of the most widely used metal oxides in catalysis, taking advantage of its mesoporous properties, textural and surface chemical properties and its high surface area.^{1,2,26–29} The low-index γ -Al₂O₃ surfaces are rich of acidic and basic sites represented in Al³⁺ ions and O²⁻ anions, respectively.²⁶ These sites are active and selective for acid–base surface reactions, including ADH. A recent experimental study by Rodemerck *et al.* has identified alumina as an effective catalyst for isobutane dehydrogenation to isobutylene.²⁸ Recent computational work revealed the dissociated H₂ binding energy (H₂ BE) to be a descriptor for C–H activation^{1,11} and dehydrogenation activity (volcano plot) on different γ -Al₂O₃ facets.¹ However, the most stable (100) γ -Al₂O₃ facet exhibited surface sites with low to moderate dehydrogenation activity.¹ Interestingly, the characteristic Lewis acid–base properties of metal oxides allow to yield promising candidates for ADH reactions. For instance, doping γ -Al₂O₃ with heterometals can open new avenues for tuning the catalytic activity *via* altering the electronic properties of the catalyst.^{29–36} As a result, much work has focused on the search for dopants as a further dimension for optimal catalyst design.

Previously, Khaleel *et al.* have experimentally doped γ -Al₂O₃ with various transition metal ions including V³⁺, Fe³⁺, Cr³⁺, Mn²⁺, and Ce³⁺, and showed that doping different ions on bulk γ -Al₂O₃ enhances the textural properties of the catalyst, including high surface area and pore volume.³³ The changes in the textural properties were mainly dependent on the nature of the dopant ion and concentration.³³ Another experimental study investigated doping γ -Al₂O₃ with three

transition metal ions, Cr³⁺, V³⁺, and Cu²⁺, and proved that doping improves the surface acidic properties of the catalyst in hydrodechlorination of 1,2-dichloroethane.³⁶ Most recently, Baklanova *et al.* have experimentally synthesized gallium-doped aluminum oxide γ -(Al_{1-x}Ga_x)₂O₃, and confirmed an enhancement of the thermodynamic stability of the doped catalyst through DFT calculations.²⁹

In this work, we apply first principles calculations to investigate the doping of γ -Al₂O₃ with gallium as a means to enhance the dehydrogenation catalytic activity. We investigate ADH of three alkanes of varying size and degree of substitution on different surface sites of Ga-doped and undoped (100) γ -Al₂O₃. It has been shown that C–H activation of light alkanes through gas-phase radical pathways is not favored on γ -Al₂O₃.^{1,37} Hence, we investigate ethane, propane, and isobutane dehydrogenation (EDH, PDH, and i-BDH, respectively) *via* two surface-stabilized competing mechanisms, namely, the concerted and stepwise. Toward accelerating the ADH catalyst discovery, we develop a universal alkane dehydrogenation model that applies fundamental properties of the catalyst and reacting hydrocarbons. Our developed methodology facilitates the screening and discovery of highly active catalysts for alkane conversion to olefins.

Computational methods

DFT calculations were performed using CP2K.³⁸ The Perdew–Burke–Ernzerhof functional³⁹ was used in conjunction with Grimme's D3 dispersion correction method.⁴⁰ This functional has been reported to produce accurate C–H activation energies on organometallic complexes when compared to higher level of theory such as Møller–Plesset perturbation theory.⁴¹ To achieve reasonable accuracy, double- ζ valence polarized basis sets were used for Al and Ga, whereas triple- ζ valence polarized basis sets were used for C, H, N, and O with the Goedecker, Teter, and Hutter pseudopotentials.^{42–45} The same combination of method and basis sets has been successfully applied to investigate propane dehydrogenation on γ -Al₂O₃.¹ All geometries were relaxed using the Broyden–Fletcher–Goldfarb–Shanno minimization algorithm until the forces converged to 4.0×10^{-4} Ha Bohr⁻¹ and an SCF convergence criterion of 10^{-8} Ha. Potential transition states of the dehydrogenation reaction profiles were located using the climbing-image nudged elastic band method⁴⁶ with a kinetic cutoff of 400 Ry, as this energetic cutoff has been shown in literature to be sufficient for calculations on γ -Al₂O₃ systems.⁴⁷ The transition states were then further optimized using the dimer method⁴⁸ and verified with vibrational frequency calculations (presence of a single imaginary vibrational mode along the reaction coordinate). The (100) surface facet of γ -Al₂O₃ was modeled using a super cell of 1×2 primitive cells containing 80 atoms (Fig. S1†). The upper four layers of the slab were allowed to relax, whereas the bottom two layers were kept frozen at their optimized bulk

positions. To avoid interactions between the periodic slabs, a vacuum space of 15 Å was set above the top layer in all calculations. The (100) Ga-doped γ -Al₂O₃ facet was constructed by replacing an Al atom with a Ga atom on the (100) γ -Al₂O₃ facet. The surface substitution energy (E_{sub}) was calculated using eqn (1):

$$E_{\text{sub}} = (E_{\text{doped surface}} + E_{\text{Al precursor}}) - (E_{\text{clean surface}} + E_{\text{Ga precursor}}) \quad (1)$$

where $E_{\text{doped surface}}$ and $E_{\text{clean surface}}$ are the total energies of the Ga-doped and clean (100) γ -Al₂O₃ surface, respectively. $E_{\text{Al precursor}}$ and $E_{\text{Ga precursor}}$ are the energies of Al and Ga precursors, respectively. In addition, the surface segregation energy (E_{seg}) was calculated as the energy difference of the metal oxide with the dopant in the surface *vs.* bulk,⁴⁹ according to eqn (2):

$$E_{\text{seg}} = (E_{\text{pure bulk}} + E_{\text{doped surface}}) - (E_{\text{doped bulk}} + E_{\text{clean surface}}) \quad (2)$$

where $E_{\text{pure bulk}}$ and $E_{\text{doped bulk}}$ are the total energies of a dopant-free bulk and the bulk structure with a single dopant, respectively. The dissociated hydrogen binding energy (H_2 BE) was computed on Lewis acid and base sites of the oxide surface,^{1,11} according to eqn (3):

$$\text{H}_2 \text{ BE} = E_{\text{Surface+H}_2} - (E_{\text{H}_2} + E_{\text{clean surface}}) \quad (3)$$

where $E_{\text{Surface+H}_2}$ is the total energy of a dissociated H_2 adsorbed on the surface, and E_{H_2} is the total energy of gas-phase H_2 . The carbenium ion stability (CIS) of the alkanes is defined as the proton affinity of the corresponding alkenes,^{2,31,50} and is calculated according to eqn (4):

$$\text{CIS} = |E_{\text{C}_n\text{H}_{2n+1}^+} - E_{\text{C}_n\text{H}_{2n}}| \quad (4)$$

where $E_{\text{C}_n\text{H}_{2n+1}^+}$ is the total energy of the carbenium ion, and $E_{\text{C}_n\text{H}_{2n}}$ is the total energy of the alkene. In this equation, the electronic energy of a proton is assumed to be zero.

Results and discussion

The nonspinel model of γ -Al₂O₃, suggested by Sautet and coworkers, was used in all the calculations.^{51,52} Computational studies have shown that the (100) γ -Al₂O₃ surface is free of water under dehydrogenation conditions with total dehydration occurring above 600 K, unlike the (110) γ -Al₂O₃ surface that is hydroxylated at temperatures between 500–1000 K.^{51–53} In addition, the surface energy of the (100) γ -Al₂O₃ is lower (more stable) than that of the fully dehydrated (110) γ -Al₂O₃ surface.^{51–53} Therefore, the nonhydroxylated (100) γ -Al₂O₃ is considered in this work. For the construction of Ga-doped (100) γ -Al₂O₃, we considered two configurations by introducing a Ga atom at two distinct pentacoordinated Al sites, namely, Al^{Va} and Al^{Vb} (Fig. 1).

Previous work revealed that H_2 BE is used to probe the strength of the Lewis acid–base site pairs and can be used as

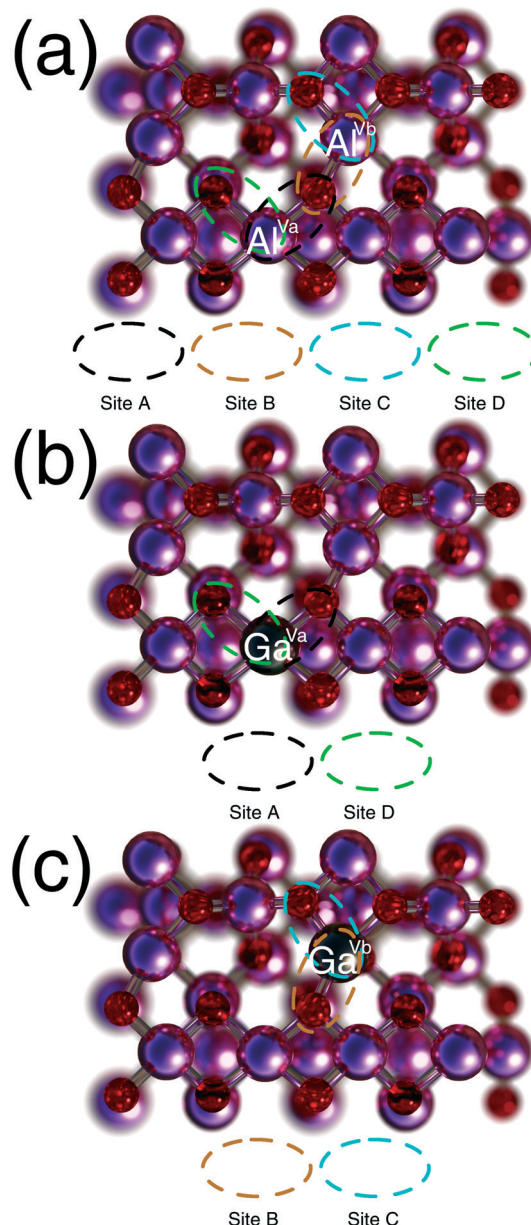


Fig. 1 Top view of different Lewis acid–base site pairs on (a) (100) γ -Al₂O₃, (b) Ga^{Va}-doped (100) γ -Al₂O₃, and (c) Ga^{Vb}-doped (100) γ -Al₂O₃. Key: Al: magenta, O: red, and Ga: black.

an activity descriptor for ADH.^{1,11} Binding of dissociated H_2 to a weak Lewis acid–base site pair implies that the physical adsorption of dissociated hydrogens is easily reversed to generate the hydrogen molecule (desorption). On the other side, adsorption on a strong Lewis acid–base site pair results in higher energetic penalties to desorb the dissociated hydrogen from the catalytic surface and may eventually poison the catalyst.^{54,55} In accordance with the Sabatier principle — that is, binding of adsorbates to the catalyst must be neither too weak nor too strong — an intermediate acid–base strength of the active sites is required for the ADH reaction. Previously, Dixit *et al.* developed a propane dehydrogenation volcano type of activity plot, where the

optimal H₂ BE on the acid–base surface pairs corresponding to high dehydrogenation rates (top of the volcano plot) was around -57 kJ mol^{-1} . Thus, to identify active sites for dehydrogenation, we calculated H₂ BE on different surface sites of Ga-doped and undoped (100) $\gamma\text{-Al}_2\text{O}_3$, as shown in Fig. 1. We found that introducing the dopant Ga atom to the (100) $\gamma\text{-Al}_2\text{O}_3$ surface, increased the H₂ BE (became more exothermic for sites A and D and less endothermic for sites B and C) (Fig. 2). This increase in the H₂ BE (stronger Lewis acid–base sites) correlates with a decrease in the C–H activation barriers which, in turn, indicates a potential improvement in the dehydrogenation activity.^{1,11} Furthermore, H₂ dissociation on Ga^{Va}-doped (100) $\gamma\text{-Al}_2\text{O}_3$ (exothermic) is thermodynamically more favored than on Ga^{Vb}-doped (100) $\gamma\text{-Al}_2\text{O}_3$ (endothermic), indicating a potential of higher catalytic activity of Ga^{Va}-doped (100) $\gamma\text{-Al}_2\text{O}_3$ toward ADH. Additionally, we noted that the calculated H₂ BE on site A doped is more exothermic ($-55.1 \text{ kJ mol}^{-1}$) than that on site D doped ($-19.6 \text{ kJ mol}^{-1}$) due to the higher Lewis basicity of the surface oxygen of site A doped. Having observed this change in the Lewis acid–base strengths of the (100) $\gamma\text{-Al}_2\text{O}_3$ sites upon doping with Ga (depicted on the H₂ BE), we investigated the ADH mechanisms of three alkanes of varying size and degree of substitution *via* the concerted and stepwise mechanisms. Specifically, we studied ADH on sites A and D in their doped and pure states due to their stronger H₂ binding (stronger Lewis acid–base pairs) compared to sites B and C. The selected site pairs on Ga^{Va}-doped (100) $\gamma\text{-Al}_2\text{O}_3$ were: Ga^{Va}-O^{IIIa} (A doped), and Ga^{Va}-O^{IIIc} (D doped), whereas those on undoped (100) $\gamma\text{-Al}_2\text{O}_3$ were: Al^{Va}-O^{IIIa} (A undoped), and Al^{Va}-O^{IIIc} (D undoped).

Fig. 3 shows graphical representations of relevant intermediates and transition states (TSs) in the concerted (Fig. 3, top panel) and stepwise (Fig. 3, bottom panel) mechanisms of ethane dehydrogenation on site A undoped of the (100) $\gamma\text{-Al}_2\text{O}_3$ facet. For the concerted pathway, the alkane is directly dehydrogenated to the corresponding olefin *via* simultaneous cleavage of two C–H bonds through a six-membered TS (TS1, Fig. 3, top panel). Then, a molecular

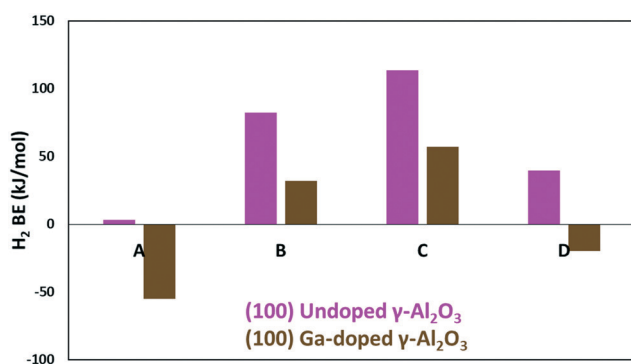


Fig. 2 H₂ BE for respective site pairs (A–D) on undoped (100) $\gamma\text{-Al}_2\text{O}_3$ (purple bars) and Ga-doped (100) $\gamma\text{-Al}_2\text{O}_3$ (brown bars). Negative values indicate exothermic adsorption.

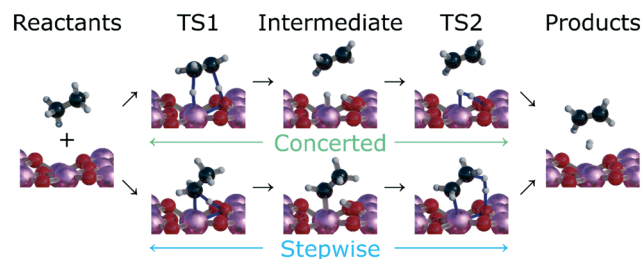


Fig. 3 Most preferred mechanisms for ethane dehydrogenation on site A undoped of the (100) $\gamma\text{-Al}_2\text{O}_3$ surface. TS1 and TS2 denote C–H activation and H₂ production transition states, respectively. Top: concerted mechanism. Bottom: stepwise mechanism. Key: Al is purple, O is red, C is black, and H is white. Transition state partial bonds are in blue.

hydrogen is formed *via* recombination of the two surface-bound hydrogens (TS2, Fig. 3, top panel). In the stepwise mechanism, the activation of the C–H bond yields a surface-bound organometallic complex (*i.e.*, compounds with metal–carbon bonds) and a neighboring hydroxyl group (TS1, Fig. 3, bottom panel). The next step is the formation of the olefin and molecular hydrogen through the recombination of the surface-bound proton and one of the β -hydrogen atoms of the alkyl fragment *via* a six-membered TS (TS2, Fig. 3, bottom panel). The catalytic cycle for both mechanisms is completed when the olefin and molecular hydrogen desorb to regenerate the catalyst.

Now we direct our attention to the reaction energetics of ethane dehydrogenation over Ga^{Va}-doped and undoped (100) $\gamma\text{-Al}_2\text{O}_3$ (Fig. 4). Propane and isobutane dehydrogenation energy profiles are reported in Fig. S2–S5 of the ESI.† The first step in both mechanisms is the weak exothermic adsorption of ethane on the active sites. We noted that physisorption of isobutane on the active sites is more exothermic ($-41.8 \text{ kJ mol}^{-1}$) than that of propane ($-36.7 \text{ kJ mol}^{-1}$) and ethane ($-27.6 \text{ kJ mol}^{-1}$) due to the increase in the molecular size and chain length.^{56,57} For the concerted mechanism, C–H activation step is energetically demanding, with calculated energy barriers of 254.8, and 292.1 kJ mol^{-1} for site A undoped and D undoped, respectively. Site A undoped exhibits lower C–H activation barrier than D undoped due to the higher Lewis basicity of the involved oxygen (both sites share the same metal center as shown in Fig. 1).^{1,11} The barrier for the subsequent step (H₂ production) is 38.3 kJ mol^{-1} for A undoped, and 98.4 kJ mol^{-1} for D undoped. These findings suggest that C–H activation is the rate determining step (RDS) for the concerted mechanism (Fig. 4(a)). To complete the catalytic cycle, ethylene and molecular hydrogen are desorbed to the gas phase to regenerate the catalytic surface. Considering doping effects, the C–H activation barriers on Ga^{Va}-doped (100) $\gamma\text{-Al}_2\text{O}_3$ were found to be 48.9 and 61.9 kJ mol^{-1} lower than those of undoped (100) $\gamma\text{-Al}_2\text{O}_3$ for sites A, and D, respectively. In conjunction, H₂ production energy barriers increased by 60.1 and 69.0 kJ mol^{-1} for sites A doped and D doped, respectively. Interestingly, we found that the dopant atom significantly decreases the RDS C–H activation barriers of the concerted mechanism.

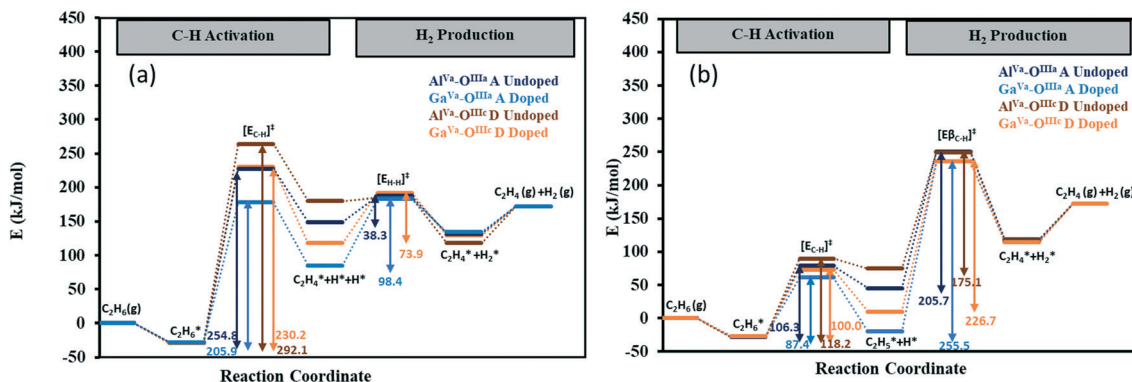


Fig. 4 Reaction energy profile of ethane dehydrogenation on Ga^{Va} -doped and undoped (100) $\gamma\text{-Al}_2\text{O}_3$ via (a) concerted and (b) stepwise mechanism at the corresponding Lewis acid–base site pairs. $E_{\text{C-H}}^{\ddagger}$ is the electronic energy of the transition state for C–H activation, whereas $E_{\text{C-H}}^{\ddagger}$ and $E_{\text{C-H}}^{\ddagger}$ are the electronic energies of the transition states for hydrogen production through the concerted mechanism and stepwise mechanism, respectively. Adsorbed states are denoted with asterisks.

In the stepwise mechanism, C–H activation exhibited lower barriers ($87\text{--}118\text{ kJ mol}^{-1}$) than those of concerted mechanism ($206\text{--}292\text{ kJ mol}^{-1}$). However, this trend was reversed in the subsequent H_2 production step. The H_2 production energy barriers were 167.4 and 157.1 kJ mol^{-1} higher than those of the concerted mechanism for sites A in undoped and Ga^{Va} -doped (100) $\gamma\text{-Al}_2\text{O}_3$, respectively. For site D, the barriers were 170.2 and 152.8 kJ mol^{-1} higher than those of the concerted mechanism for D undoped and D doped, respectively. As a result, the H_2 production step is the RDS in the stepwise mechanism (Fig. 4(b)). The change in the energy barriers could be attributed to the higher electronegativity of Ga atom compared to Al atom, with the Ga doped active sites being more acidic than the undoped sites.

As noted earlier, H_2 BE is an activity descriptor for ADH and can probe the strength of the Lewis acid–base site pairs.^{1,11} Thus, we plotted H_2 BE against dehydrogenation energy barriers for the concerted and stepwise mechanisms. Fig. 5 shows the correlation between the H_2 BE and the transition state barriers for C–H activation (Fig. 5(a)) and H_2 production (Fig. 5(b)) steps of the concerted mechanism (preferred mechanism, *vide infra*). The equivalent correlations for C–H activation and H_2 production of the stepwise mechanism are shown in Fig. S6 and S7,[†] respectively. A very good correlation was found between H_2 BE and the activation energies of the two steps of the concerted mechanism (Fig. 5). Our calculations showed that strong Lewis acid–base site pairs with strong H_2 BE exhibit low C–H activation barriers, whereas weak Lewis acid–base sites exhibit low H_2 production barriers, in agreement with previous ADH structure–activity relations (SARs) study on $\gamma\text{-Al}_2\text{O}_3$.^{1,11} We noted that the equivalent correlations of the stepwise mechanism (Fig. S6 and S7[†]) are relatively weaker than those of the concerted mechanism (Fig. 5). In the H_2 production step of the stepwise mechanism, the weaker correlation can be attributed to the participation of only the basic site (surface oxygen) in the production of the molecular H_2 . However, in the concerted mechanism, both dual active sites (surface Al and oxygen atoms) participate in the H_2

production step. Importantly, the results of Fig. 5 demonstrate that the H_2 BE can be a descriptor for Lewis acid/base properties of surface pair sites on mixed (doped) metal oxides in addition to pure oxides.

To examine the effect of alkane size and degree of substitution, the CIS was plotted against the C–H activation

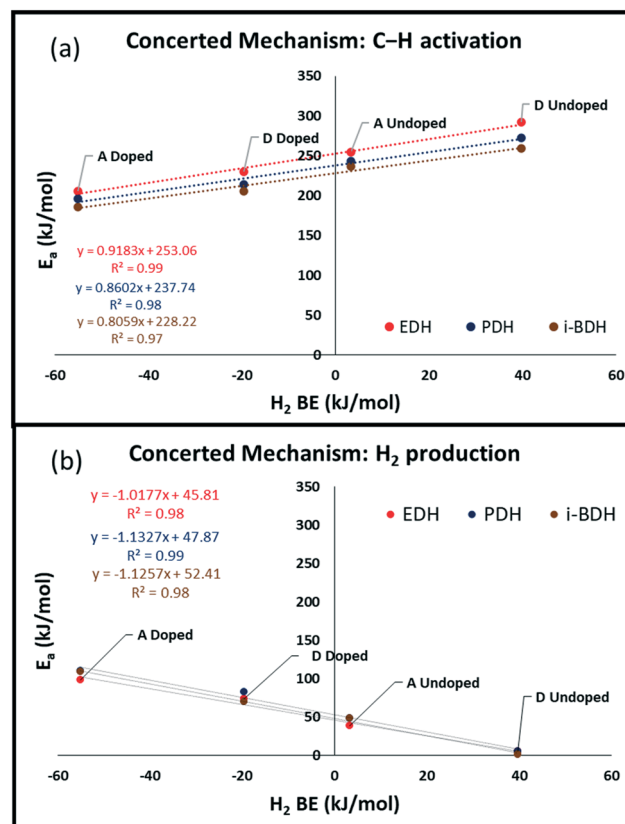


Fig. 5 Dehydrogenation barriers on Ga^{Va} -doped and undoped (100) $\gamma\text{-Al}_2\text{O}_3$ vs. H_2 BE on the corresponding Lewis acid–base site pairs for (a) C–H activation and (b) H_2 production of the concerted mechanism. Red, blue, and brown circles correspond to ethane – EDH, propane – PDH, and isobutane – i-BDH dehydrogenation, respectively.

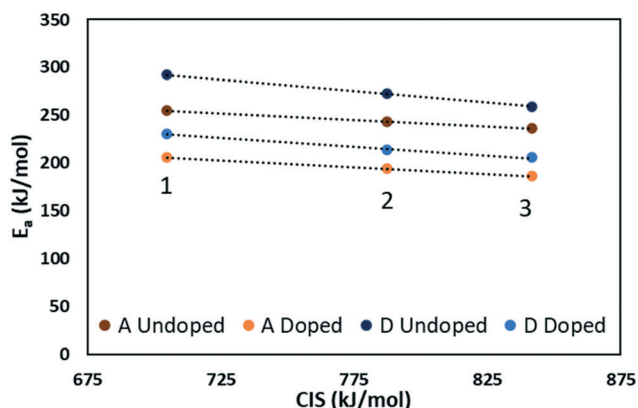


Fig. 6 DFT-calculated C–H activation energy barriers vs. CIS for the concerted mechanism at the respective acid–base site pairs. Data points corresponding to primary, secondary, and tertiary carbocation intermediates are denoted with numerical insets (primary: 1, secondary: 2, tertiary: 3).

(RDS) barriers of the concerted pathway (Fig. 6), where higher CIS values indicate higher stability and correspond to higher degree of alkane substitution. We found an inverse relationship between CIS and the C–H activation barriers; C–H activation barriers decrease as the alkane size and degree of substitution increase, with *i*-BDH exhibiting the lowest C–H activation barriers at all respective site pairs. The presence of additional methyl groups in isobutane compared to ethane and propane, resulted in higher stability of the reaction intermediate.² The corresponding correlation between the dehydrogenation barriers of the RDS for the stepwise mechanism and CIS is shown in Fig. S8.† Importantly, we show the CIS being a quantitative descriptor in ADH, correlating with the calculated TS energy barriers for alkanes of different substitution. The CIS cannot describe the H₂ production step of the concerted mechanism simply because the respective TS does not involve the alkane. Instead, the TS involves properties of the Lewis acid–base site pair (H₂ is formed through recombination of the two surface-bound hydrogens).

Previously, Kostetsky *et al.* developed an alkane dehydrogenation model for the kinetically preferred concerted mechanism.² This model applies three physicochemical properties that include: CIS, alkane binding energy, and proton affinity as descriptors for alkane stability, and catalyst acidity and basicity. Similarly, using a methodology previously applied in SARs for alkane dehydrogenation and alcohol dehydration,^{2,31,58} we developed an alkane dehydrogenation model for the RDSs of the concerted and stepwise mechanisms (C–H activation and H₂ production steps of Fig. 4(a) and (b), respectively). Our model applies the H₂ BE as a descriptor for the catalyst acidity and basicity (as shown in Fig. 5) and the CIS as a descriptor for reactant substitution (as shown in Fig. 6). The model was developed by performing a multi-parameter linear regression of the calculated DFT dehydrogenation barriers of the three alkanes in question (model details are shown in Tables S1 and S2†). A very good agreement can be observed between DFT-calculated and model-predicted dehydrogenation values of the RDS for the concerted and stepwise mechanisms (Fig. 7). The model was further verified with leave one out cross validation with mean square error of 15.2 kJ mol⁻¹ for the concerted mechanism model and 6.4 kJ mol⁻¹ for the stepwise mechanism model. The flexibility of the dehydrogenation model relies on the use of fundamental descriptors which could be easily calculated for different alkanes and oxide sites. As a result, our dehydrogenation model facilitates the prediction of the activation energy of alkane dehydrogenation on group IIIA metal oxides, in their doped and undoped states. Hence, the model could be used as a useful tool to screen group IIIA metal oxides toward the selective formation of olefins from different alkanes.

Toward obtaining catalytic activity trends, we calculated the overall turnover frequencies (TOFs) of the three different dehydrogenation reactions at a typical Catofin temperature of 873 K,^{1,3} based on the energetic span model.⁵⁹ By plotting the highest TOFs for the selected acid–base site pairs against H₂ BE, we identified H₂ BE as a quantitative descriptor in ADH to predict the overall TOFs. We confirmed that doping

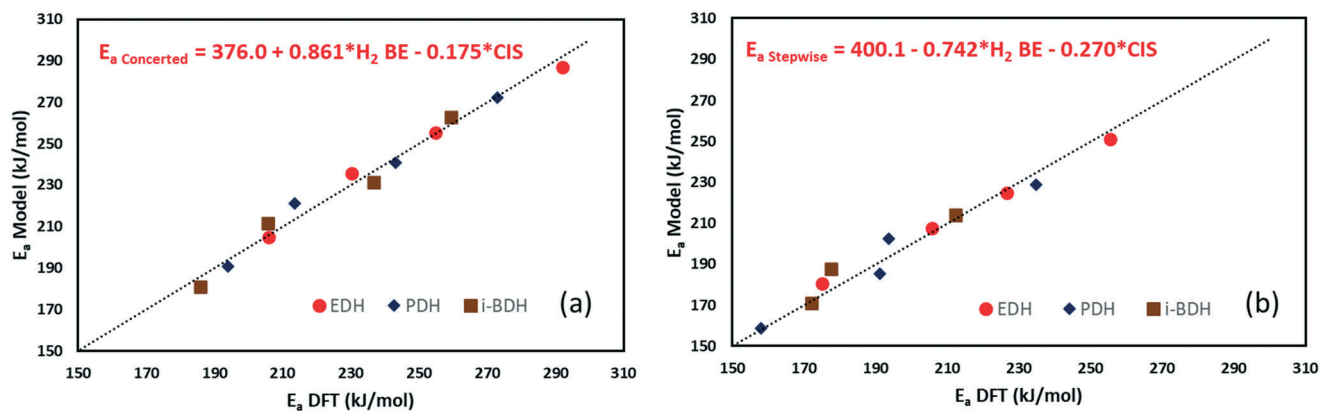


Fig. 7 Parity plot of model-predicted and DFT calculated dehydrogenation barriers for the RDSs of (a) concerted and (b) stepwise mechanisms of ethane – EDH (red circles), propane – PDH (blue diamond), and isobutane – *i*-BDH (brown squares). The alkane dehydrogenation model expression is shown as inset to the figures.

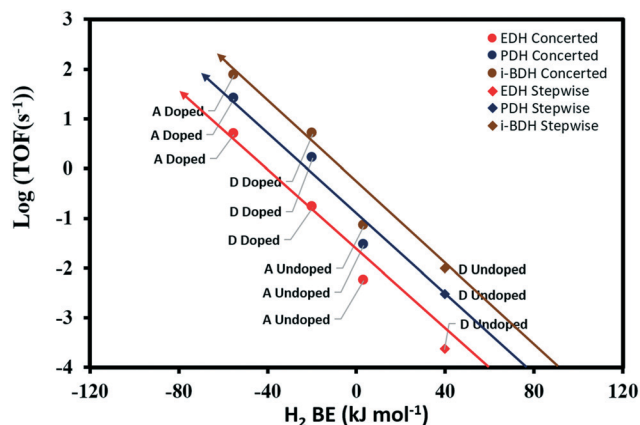


Fig. 8 Log (TOF) of ethane (red), propane (blue), and isobutane (brown) dehydrogenation reactions at different site pairs for the most preferred mechanism (highest TOFs) vs. H_2 BE. Circles denote preference for concerted mechanism and diamond for stepwise mechanism.

Al^{Va} with Ga significantly enhances the catalytic activity by increasing the TOFs of the different ADH reactions (Fig. 8). Additionally, we noted that the highly-substituted alkanes achieve higher dehydrogenation rates. Our calculations identified that out of the different studied Lewis acid–base site pairs, site A doped is the most active site for ADH, exhibiting the highest TOFs for all ADH reactions. Going back to the H_2 BE results of Fig. 2, this finding demonstrates that acid–base pair sites that bind mildly H_2 are needed to exhibit enhanced dehydrogenation activity while not poisoning the catalyst surface.¹ We found the concerted mechanism to be the kinetically most preferred mechanism over most of the acid–base sites. Table S3† reports the energies of the TOF-determining transition state (TDTS) and TOF-determining intermediate (TDI) for all three ADH reactions. For site D undoped, the TDTS of the stepwise mechanism was more stable than that of the concerted, therefore, the stepwise mechanism was kinetically preferred over the concerted mechanism.

Finally, to address the synthetic accessibility of Ga^{Va} -doped (100) $\gamma-Al_2O_3$, we calculated the substitution energy according to eqn (1), where the gas phase Ga atom was used as a reference. We found that the substitutional doping is highly endothermic with an energy of 335 kJ mol^{-1} . However, we note that experimental studies on substitutional doping, use metal salts as the precursor species.^{29,33,36} For instance, gallium nitrate has been experimentally used as a Ga precursor to synthesize Ga-doped catalysts.²⁹ Thus, using gallium nitrate as a reference, we found that the substitutional doping became effectively thermoneutral (2.7 kJ mol^{-1}). In addition, the substitutional free energy was calculated under a typical Catofin temperature of 873 K. The calculation demonstrated a highly exothermic substitution ($-424.3 \text{ kJ mol}^{-1}$), confirming the possibility of incorporating Ga into the (100) $\gamma-Al_2O_3$ surface with the choice of an appropriate precursor. Finally, we also computed the surface segregation energy and found that segregation to the surface is thermodynamically favored (-75.8

kJ mol^{-1}). The rationale behind the surface segregation preference is the metal atomic size.⁴⁹ The dopant atom (Ga) has a larger atomic radius compared to that of the host atom (Al), leading to strain occurrence when Ga is doped in the bulk of $\gamma-Al_2O_3$. To release this strain, the dopant atom prefers to segregate to the surface.

Conclusion

We employed first principles calculations to investigate the nonoxidative dehydrogenation of ethane, propane, and isobutane on Ga^{Va} -doped and undoped (100) $\gamma-Al_2O_3$ through the concerted and stepwise mechanisms. Our results demonstrated that doping (100) $\gamma-Al_2O_3$ with Ga significantly improves the catalytic activity by decreasing the C–H activation energy barriers of the kinetically favored concerted mechanism and increasing the overall dehydrogenation turnover frequencies. We identified the dissociated H_2 binding energy as a quantitative dehydrogenation activity descriptor, accounting for the strength of the catalyst Lewis acidity and basicity. We found a linear relationship between the dissociated H_2 binding energy and the energy barrier of the rate determining steps of the concerted and stepwise mechanisms. Further, we demonstrated that the alkane size and degree of substitution have a clear effect on the dehydrogenation activity, with highly-substituted alkanes exhibiting lower dehydrogenation barriers for the concerted mechanism. Importantly, we developed an alkane dehydrogenation model that uses fundamental physicochemical properties of the catalyst to predict the dehydrogenation performance on different oxide surface sites. With the dissociated H_2 binding energy governing the dehydrogenation activity, we revealed that this descriptor can be used to predict the overall dehydrogenation turnover frequencies. Finally, our calculations revealed that Ga^{Va} -doped (100) $\gamma-Al_2O_3$ surface is an active surface for nonoxidative alkane dehydrogenation and can be experimentally accessed by doping $\gamma-Al_2O_3$ through the use of appropriate Ga-precursors. Overall, our developed methodology accelerates the screening of metal oxides toward nonoxidative alkane dehydrogenation and introduces promising routes (doping) to enhance catalytic activity.

Conflicts of interest

There are no conflicts of interest to declare.

Acknowledgements

This work was supported by the National Science Foundation (NSF), under grant no. 1920623. The authors would like to acknowledge computational support from the Center for Research Computing (CRC) at the University of Pittsburgh and the Extreme Science and Engineering Discovery Environment (XSEDE), which is supported by the NSF (ACI-1548562).

References

- M. Dixit, P. Kostetsky and G. Mpourmpakis, *ACS Catal.*, 2018, **8**, 11570–11578.
- P. Kostetsky, C. M. Nolan, M. Dixit and G. Mpourmpakis, *Ind. Eng. Chem. Res.*, 2018, **57**, 16657–16663.
- J. J. H. B. Sattler, J. Ruiz-Martinez, E. Santillan-Jimenez and B. M. Weckhuysen, *Chem. Rev.*, 2014, **114**, 10613–10653.
- A. J. L. Pombeiro and M. F. C. Guedes da Silva, *Alkane Functionalization*, John Wiley & Sons, 2018.
- I. Amghizar, L. A. Vandewalle, K. M. Van Geem and G. B. Marin, *Engineering*, 2017, **3**, 171–178.
- S. M. Sadrameli, *Fuel*, 2015, **140**, 102–115.
- Y. Liu, Z. H. Li, J. Lu and K.-N. Fan, *J. Phys. Chem. C*, 2008, **112**, 20382–20392.
- F. Cavani, N. Ballarini and A. Cericola, *Catal. Today*, 2007, **127**, 113–131.
- O. Ovsitser, R. Schomaecker, E. V. Kondratenko, T. Wolfram and A. Trunschke, *Catal. Today*, 2012, **192**, 16–19.
- J. E. Germain, Academic Press, 1969.
- M. C. Cholewinski, M. Dixit and G. Mpourmpakis, *ACS Omega*, 2018, **3**, 18242–18250.
- E. Araujo-Lopez, L. Joos, B. D. Vandegheuchte, D. I. Sharapa and F. Studt, *J. Phys. Chem. C*, 2020, **124**, 3171–3176.
- E. C. Tyo, C. Yin, M. Di Vece, Q. Qian, G. Kwon, S. Lee, B. Lee, J. E. DeBartolo, S. N. Seifert, R. E. Winans, R. Si, B. Ricks, S. Goergen, M. Rutter, B. Zugic, M. Flytzani-Stephanopoulos, Z. W. Wang, R. E. Palmer, M. Neurock and S. Vajda, *ACS Catal.*, 2012, **2**, 2409–2423.
- L. Cheng, G. A. Ferguson, S. A. Zymunt and L. A. Curtiss, *J. Catal.*, 2013, **302**, 31–36.
- V. Fung, F. F. Tao and D.-e. Jiang, *J. Phys. Chem. Lett.*, 2017, **8**, 2206–2211.
- G. Fu, Z.-N. Chen, X. Xu and H.-L. Wan, *J. Phys. Chem. A*, 2008, **112**, 717–721.
- C. Coperet, *Chem. Rev.*, 2010, **110**, 656–680.
- M. A. Bañares, *Catal. Today*, 1999, **51**, 319–348.
- P. Michorczyk and J. Ogonowski, *React. Kinet. Catal. Lett.*, 2003, **78**, 41–47.
- G. R. Jenness, M. A. Christiansen, S. Caratzoulas, D. G. Vlachos and R. J. Gorte, *J. Phys. Chem. C*, 2014, **118**, 12899–12907.
- S. Roy, G. Mpourmpakis, D.-Y. Hong, D. G. Vlachos, A. Bhan and R. J. Gorte, *ACS Catal.*, 2012, **2**, 1846–1853.
- M. A. Christiansen, G. Mpourmpakis and D. G. Vlachos, *ACS Catal.*, 2013, **3**, 1965–1975.
- J. J. H. B. Sattler, I. D. Gonzalez-Jimenez, L. Luo, B. A. Stears, A. Malek, D. G. Barton, B. A. Kilos, M. P. Kaminsky, M. W. G. M. Verhoeven, E. J. Koers, M. Baldus and B. M. Weckhuysen, *Angew. Chem., Int. Ed.*, 2014, **53**, 9251–9256.
- J. Qu, S. C. E. Tsang and X.-Q. Gong, *J. Mol. Model.*, 2014, **20**, 1–9.
- E. A. Pidko, E. J. M. Hensen and R. A. van Santen, *J. Phys. Chem. C*, 2007, **111**, 13068–13075.
- H. Knözinger and P. Ratnasamy, *Catal. Rev.: Sci. Eng.*, 1978, **17**, 31–70.
- L. Evenäs, I. Furó, P. Stilbs and R. Valiullin, *Langmuir*, 2002, **18**, 8096–8101.
- U. Rodemerck, E. V. Kondratenko, T. Otroshchenko and D. Linke, *Chem. Commun.*, 2016, **52**, 12222–12225.
- I. V. Baklanova, V. N. Krasil'nikov, A. P. Tyutyunnik, A. N. Enyashin, Y. V. Baklanova, O. I. Gyrdasova, R. F. Samigullina and E. G. Vovkotrub, *Spectrochim. Acta, Part A*, 2020, **227**, 117658.
- X. Qiu, J. Zhang, H. Dong and X. Zhou, *Theor. Chem. Acc.*, 2017, **136**, 1–7.
- P. Kostetsky and G. Mpourmpakis, *Catal. Sci. Technol.*, 2015, **5**, 4547–4555.
- Y. Ma, X. Zhao, M. Niu, W. Li, X. Wang, C. Zhai, T. Wang, Y. Tang and X. Dai, *RSC Adv.*, 2017, **7**, 4124–4134.
- A. Khaleel, M. Nawaz, S. Al-Hadrami, Y. Greish and T. Saeed, *Microporous Mesoporous Mater.*, 2013, **168**, 7–14.
- T. Wang, F. Jiang, G. Liu, L. Zeng, Z. J. Zhao and J. Gong, *AIChE J.*, 2016, **62**, 4365–4376.
- M. Chen, J. Xu, F.-Z. Su, Y.-M. Liu, Y. Cao, H.-Y. He and K.-N. Fan, *J. Catal.*, 2008, **256**, 293–300.
- A. Khaleel and M. Nawaz, *J. Environ. Sci.*, 2015, **29**, 199–209.
- J. Joubert, F. Delbecq and P. Sautet, *J. Catal.*, 2007, **251**, 507–513.
- J. VandeVondele, M. Krack, F. Mohamed, M. Parrinello, T. Chassaing and J. Hutter, *Comput. Phys. Commun.*, 2005, **167**, 103–128.
- J. P. Perdew, K. Burke and M. Ernzerhof, *Phys. Rev. Lett.*, 1997, **78**, 1396.
- S. Grimme, *J. Comput. Chem.*, 2006, **27**, 1787–1799.
- E. S. Xavier, W. R. Rocha and W. B. De Almeida, *Chem. Phys. Lett.*, 2006, **430**, 160–166.
- J. VandeVondele and J. Hutter, *J. Chem. Phys.*, 2007, **127**, 114105.
- S. Goedecker, M. Teter and J. Hutter, *Phys. Rev. B: Condens. Matter Mater. Phys.*, 1996, **54**, 1703.
- C. Hartwigsen, S. Goedecker and J. Hutter, *Phys. Rev. B: Condens. Matter Mater. Phys.*, 1998, **58**, 3641.
- M. Krack, *Theor. Chem. Acc.*, 2005, **114**, 145.
- G. Henkelman, B. P. Uberuaga and H. Jónsson, *J. Chem. Phys.*, 2000, **113**, 9901–9904.
- R. Réocreux, T. Jiang, M. Iannuzzi, C. Michel and P. Sautet, *ACS Appl. Nano Mater.*, 2018, **1**, 191–199.
- G. Henkelman and H. Jónsson, *J. Chem. Phys.*, 1999, **111**, 7010–7022.
- L. Farsi and N. A. Deskins, *Phys. Chem. Chem. Phys.*, 2019, **21**, 23626–23637.
- P. Kostetsky, J. P. Maheswari and G. Mpourmpakis, *J. Phys. Chem. C*, 2015, **119**, 16139–16147.
- M. Digne, P. Sautet, P. Raybaud, P. Euzen and H. Toulhoat, *J. Catal.*, 2004, **226**, 54–68.
- M. Digne, P. Sautet, P. Raybaud, P. Euzen and H. Toulhoat, *J. Catal.*, 2002, **211**, 1–5.
- R. Wischert, P. Laurent, C. Copéret, F. O. Delbecq and P. Sautet, *J. Am. Chem. Soc.*, 2012, **134**, 14430–14449.

- 54 P. A. Webb, Micromeritics Instrument Corp., Technical Publications, 2003.
- 55 P. Lamoureux, *Computational Modeling in Heterogeneous Catalysis*, 2017.
- 56 B. A. Sexton and A. E. Hughes, *Surf. Sci.*, 1984, **140**, 227–248.
- 57 A. V. Teplyakov, A. B. Gurevich, M. X. Yang, B. E. Bent and J. G. Chen, *Surf. Sci.*, 1998, **396**, 340–348.
- 58 P. Kostestky, J. Yu, R. J. Gorte and G. Mpourmpakis, *Catal. Sci. Technol.*, 2014, **4**, 3861–3869.
- 59 S. Kozuch and S. Shaik, *Acc. Chem. Res.*, 2011, **44**, 101–110.